Supplementary material

Synthesis, Crystal Structure, Thermal Decomposition and ^{11}B MAS NMR Characterization of $Mg(BH_4)_2(NH_3BH_3)_2$

Lars H. Jepsen[a], Voraksmy Ban[b], Kasper T. Møller[a], Young-Su Lee[c], Young Whan Cho[c], Flemming Besenbacher[d], Yaroslav Filinchuk[b], Jørgen Skibsted[e] and Torben R. Jensen[a*]

[a]*Center for Materials Crystallography, Interdisciplinary Nanoscience Center and Department of Chemistry, Aarhus University, Langelandsgade 140, DK-8000 Aarhus C, Denmark*

[b] *Institute of Condensed Matter and Nanosciences, Université catholique de Louvain, Place L. Pasteur 1, B-1348, Louvain-la-Neuve, Belgium*

[c] *High Temperature Energy Materials Research Center, Korea Institute of Science and Technology, Seoul 136-791, Republic of Korea*

[d] *Interdisciplinary Nanoscience Center (iNANO) and Department of Physics and Astronomy, Aarhus University, Ny Munkegade 120, DK-8000 Aarhus C, Denmark.*

[e] *Instrument Centre for Solid-State NMR Spectroscopy, Department of Chemistry and Interdisciplinary Nanoscience Center (iNANO), Aarhus University, Langelandsgade 140, DK-8000 Aarhus C, Denmark*

*Corresponding author
Torben R. Jensen, Ph.D., Associate Professor
Center for Materials Crystallography
iNANO and Department of Chemistry
Langelandsgade 140
DK-8000 Aarhus C
Aarhus University
Denmark

Table S1 Experimental structural parameters for $Mg(BH_4)_2(NH_3BH_3)_2$, space group $P2_12_12_1$ (No. 19), a = 14.41633(7), b = 13.21283(7), c = 5.11512(2) Å and V = 974.331(8) Å^3

Atom	Wyckoff site	x	y	z	Occupancy	B (Å²)
Mg1	4*a*	0.88155(19)	0.2570(2)	0.0430(3)	1	3.92(5)
B2	4*a*	0.0002(4)	0.3681(4)	0.1995(12)	1	4.12(11)
H3	4*a*	0.0767(10)	0.344(2)	0.254(8)	1	2.0(2)
H4	4*a*	-0.001(2)	0.4580(7)	0.179(6)	1	2.0(2)
H5	4*a*	-0.021(2)	0.334(2)	-0.006(3)	1	2.0(2)
H6	4*a*	-0.0521(17)	0.344(2)	0.371(4)	1	2.0(2)
B7	4*a*	0.7380(4)	0.8430(4)	0.7524(13)	1	4.12(11)
H8	4*a*	0.8115(13)	0.806(2)	0.822(6)	1	2.0(2)
H9	4*a*	0.741(2)	0.855(2)	0.520(2)	1	2.0(2)
H10	4*a*	0.6807(17)	0.7817(19)	0.818(6)	1	2.0(2)
H11	4*a*	0.712(2)	0.9221(13)	0.855(4)	1	2.0(2)
N12	4*a*	0.6845(3)	0.3614(3)	0.7406(10)	1	6.36(13)
B13	4*a*	0.7860(4)	0.3868(4)	0.8288(11)	1	4.12(11)
H14	4*a*	0.677(2)	0.363(2)	0.5454(19)	1	2.0(2)
H15	4*a*	0.667(2)	0.2942(12)	0.809(5)	1	2.0(2)
H16	4*a*	0.789(2)	0.398(2)	1.063(2)	1	2.0(2)
H17	4*a*	0.8361(18)	0.3170(16)	0.758(8)	1	2.0(2)
H18	4*a*	0.8095(18)	0.4623(16)	0.712(6)	1	2.0(2)
H19	4*a*	0.642(2)	0.4104(18)	0.834(5)	1	2.0(2)
N20	4*a*	0.5829(3)	0.9825(4)	0.2814(10)	1	6.36(13)
B21	4*a*	0.5247(4)	0.8820(4)	0.3418(11)	1	4.12(11)
H22	4*a*	0.6507(8)	0.966(2)	0.287(8)	1	2.0(2)
H23	4*a*	0.570(2)	1.010(2)	0.103(3)	1	2.0(2)
H24	4*a*	0.4452(11)	0.880(2)	0.267(8)	1	2.0(2)
H25	4*a*	0.567(2)	0.8142(17)	0.229(7)	1	2.0(2)
H26	4*a*	0.521(2)	0.870(2)	0.576(2)	1	2.0(2)
H27	4*a*	0.571(2)	1.026(2)	0.432(4)	1	2.0(2)

Detailed description of structure solution and refinement The structure of the complex $Mg(BH_4)_2(NH_3BH_3)_2$ was solved and refined from SR-PXD data measured at Diamond, UK. The final Rietveld refinement (see Figure 1) indicated that the sample contains $Mg(BH_4)_2(NH_3BH_3)_2$ (86 wt%), α-$Mg(BH_4)_2$ (10 wt%) and 4 wt% of remaining NH_3BH_3.

The diffraction data from the new compound, $Mg(BH_4)_2(NH_3BH_3)_2$, were indexed with an orthorhombic unit cell, a = 14.41633(7), b = 13.21283(7), c = 5.11512(2) Å and V = 974.331(8) Å^3, using EXPO 2011.[1] The systematic absences suggested the presence of glide planes, *i.e.* *Pna*2_1 or *Pnam* (Z = 4) as the most likely space groups. However, close examination shows that a number of weak reflections (*e.g.* 301, 021, 041) break both systematic absence conditions. The structure was solved in the space group $P2_12_12_1$, using global optimization in direct space implemented in the program FOX.[2] One Mg, two rigid tetrahedral BH_4^- anions and two rigid NH_3BH_3 molecules were optimized using B─B 3.3 Å, N─N 2.5 Å and H─H 1.8 Å antibump restraints.

The structural model, shown in Table S1, was refined by the Rietveld method using the program Fullprof.[3] 81 atomic coordinates (7 non-H and 20 H-atoms) and 4 group isotropic atomic displacement factors were refined with 22 distance and 36 angle restraints (B-H distance 1.22 Å, N-H distances 1.00 Å and B-N 1.56 Å distances, all sp^3 angles are fixed at 109.5°). Intensities of 1020 independent reflections were used, which are equivalent to 330 independent observations, accounting for the effective angular resolution of the diffraction data. The observation/parameter ratio is thus highly satisfactory, exceeding 4.5. The structure was checked for higher symmetry using ADDSYM routine in Platon.[4] The final discrepancy factors: R_p = 0.66 %, R_{wp} = 0.97 % (not corrected for background), R_p = 14.1 %, R_{wp} = 8.4 % (conventional Rietveld R-factors), R_{Bragg} = 6.1 % and global χ^2 = 28.9.

Table S2. Geometrical characteristics of the shortest dihydrogen bonds in $Mg(BH_4)_2(BH_3NH_3)_2$ solved from SR-PXD.

Intermolecular									
H···H	(Å)	B-H	(Å)	N-H	(Å)	B-H···H	(deg)	N-H···H	(deg)
H4···H23	1.84(4)	B2-H4	1.19	N20-H23	1.00	B2-H4···H23	106	N20-H23···H4	154
H4···H27	2.25(4)	B2-H4	1.19	N20-H27	0.98	B2-H4···H27	90	N20-H27···H4	146
H3···H15	2.28(3)	B2-H3	1.18	N12-H15	0.98	B2-H3···H15	136	N12-H15···H3	144
Intramolecular									
H···H									
H9···H22	2.29(4)	B7-H9	1.20	N20-H22	1.00	B7-H9···H22	125	N20-H22···H9	108

Table S3 Bond distances from the refined DFT structure of $Mg(BH_4)_2(NH_3BH_3)_2$ compared with those from the reported pristine NH_3BH_3 and α-$Mg(BH_4)_2$.

Bond	**Length (Å)**		
	$Mg(BH_4)_2(NH_3BH_3)_2$	NH_3BH_3 [5]	α-$Mg(BH_4)_2$ [6]
Intramolecular			
N–B	1.577 – 1.591	1.58(2)	
N–H (NH_3BH_3)	1.026 – 1.033	0.96(3) – 1.07(4)	
B–H (NH_3BH_3)	1.207 – 1.234	1.15(3) – 1.18(3)	
B–H (BH_4)	1.216 – 1.247		1.18(1)
Mg–B	2.389 – 2.475		2.31(3) – 2.53(2)
Mg–H (BH_4)(BH_3)	1.971 – 2.074		1.81(4) – 2.25(5)
$H^{\delta+}$(NH_3BH_3)–$H^{\delta-}$(NH_3BH_3)	2.063 – 2.458	2.02(3)	
Intermolecular			
$H^{\delta+}$(NH_3BH_3)–$H^{\delta-}$(BH_4)	1.957 – 2.445		

Table S4 DFT-optimized atomic positions for $Mg(BH_4)_2(NH_3BH_3)_2$. The experimental cell parameters from SR-PXD are used.

Atom	Wyckoff site	Occupancy	*x*	*y*	*z*
Mg1	4*a*	1	0.8816	0.2518	0.0350
B2	4*a*	1	0.0023	0.3613	0.1901
H3	4*a*	1	0.0779	0.3413	0.2821
H4	4*a*	1	-0.0132	0.4521	0.1796
H5	4*a*	1	0.0007	0.3270	0.9654
H6	4*a*	1	-0.0572	0.3231	0.3336
B7	4*a*	1	0.7395	0.8503	0.7140
H8	4*a*	1	0.8154	0.8151	0.7640
H9	4*a*	1	0.7263	0.8402	0.4745
H10	4*a*	1	0.6810	0.8038	0.8459
H11	4*a*	1	0.7304	0.9397	0.7653
N12	4*a*	1	0.6800	0.3526	0.7449
B13	4*a*	1	0.7826	0.3817	0.8315
H14	4*a*	1	0.6681	0.3700	0.5524
H15	4*a*	1	0.6649	0.2768	0.7671
H16	4*a*	1	0.7880	0.3702	0.0695
H17	4*a*	1	0.8362	0.3264	0.7092
H18	4*a*	1	0.7993	0.4687	0.7768
H19	4*a*	1	0.6310	0.3907	0.8531
N20	4*a*	1	0.5757	0.9953	0.3187
B21	4*a*	1	0.5253	0.8908	0.3630
H22	4*a*	1	0.6471	0.9918	0.3223
H23	4*a*	1	0.5576	0.0275	0.1425
H24	4*a*	1	0.4438	0.8970	0.3035
H25	4*a*	1	0.5618	0.8265	0.2219
H26	4*a*	1	0.5311	0.8696	0.5969
H27	4*a*	1	0.5580	0.0468	0.4621

Table S5 Frequencies observed in FTIR for $Mg(BH_4)_2(NH_3BH_3)_2$ compared with NH_3BH_3 and α-$Mg(BH_4)_2$.

	$Mg(BH_4)_2(NH_3BH_3)_2$	NH_3BH_3	α-$Mg(BH_4)_2$
N–H strech:	3307	3304	
	3250	3248	
	3176-3213 (w, broad)	3192	
B–H strech:	2471	2313	2274
	2397	2283	
	2299	2210	
	2247	2113	
	2182		
Fingerprint:	1604	1595	1252
	1419	1372	1118
	1394	1155	
	1351	1052	
	1134		
	1043		

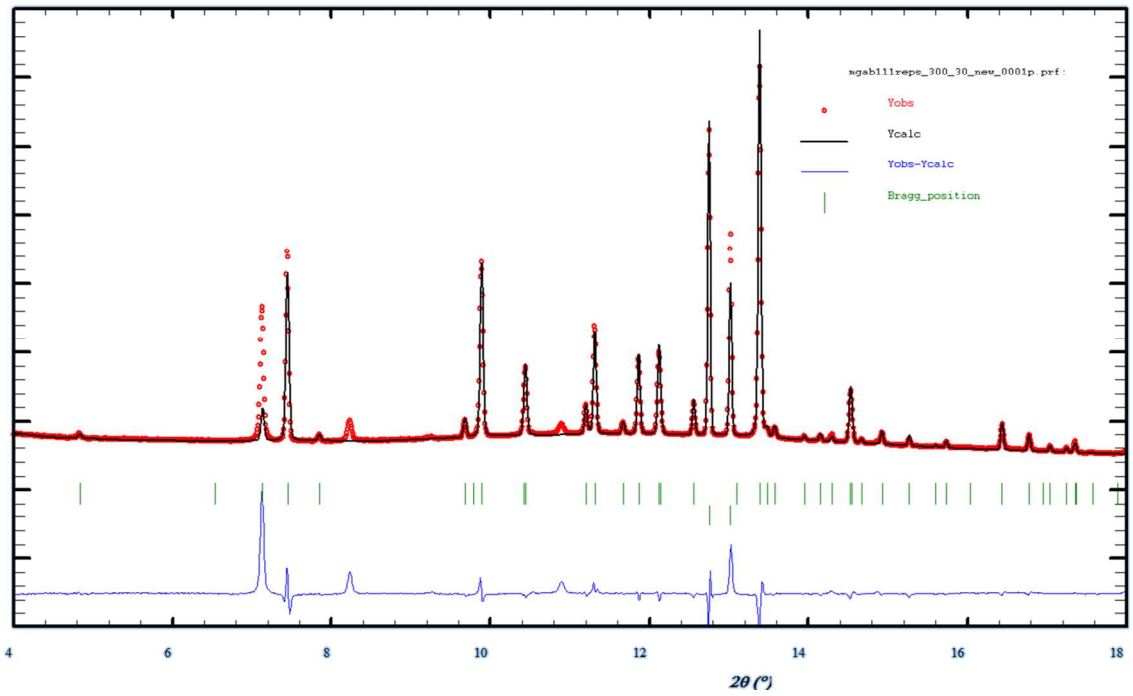

Figure S1 Rietveld refinement of SR-PXD data for α-$Mg(BH_4)_2$-NH_3BH_3 (1:2, s2) after 325 min BM measured at RT, λ = 0.823065 Å. Tic marks (top) $Mg(BH_4)_2(NH_3BH_3)_2$ and NH_3BH_3. New reflections from **2** are observed at 2θ = 7.11, 8.23, 10.90 and 13.01 °.

Figure S2 Picture of a vial containing $Mg(BH_4)_2(NH_3BH_3)_2$ in argon atmosphere stored at RT for several weeks. The powder has transformed into foam.

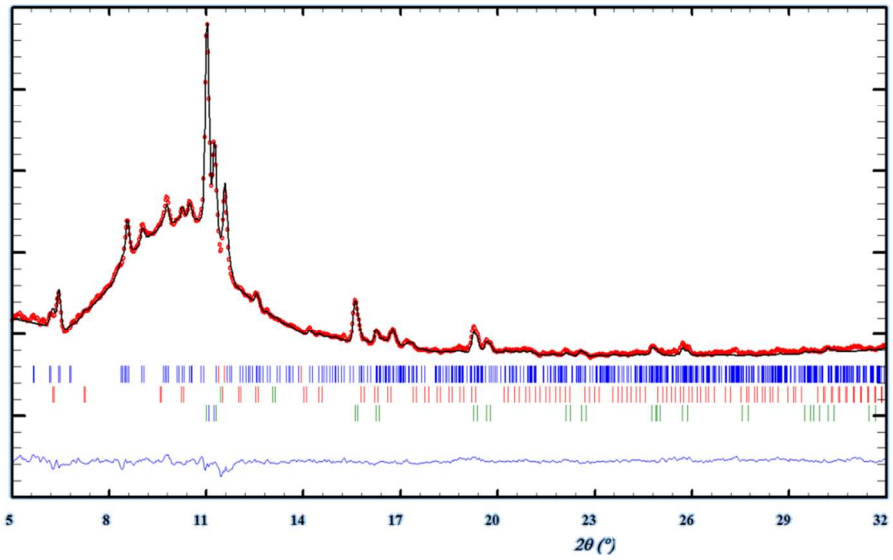

Figure S3 Rietveld refinement of PXD data for γ-$Mg(BH_4)_2$–NH_3BH_3 (1:0.66, s6) manually ground before compression, λ = 0.71073 Å, RT. Tic marks in blue show Bragg positions of $Mg(BH_4)_2(NH_3BH_3)_2$ (50 wt%), in red γ-$Mg(BH_4)_2$ (2 wt%) and in green NH_3BH_3 (48 wt%).

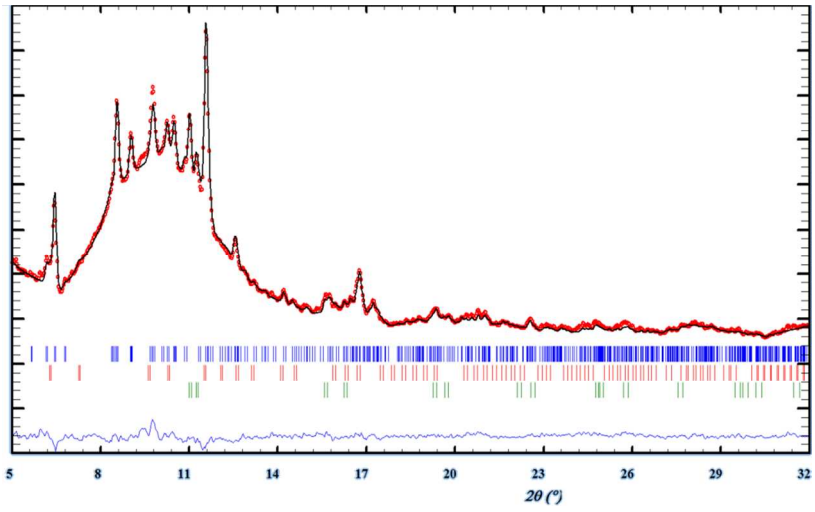

Figure S4 Rietveld refinement of PXD data for γ-$Mg(BH_4)_2$–NH_3BH_3 (1:0.66, s6) compressed into a pellet, λ = 0.71073 Å, RT. Tic marks in blue show Bragg positions of $Mg(BH_4)_2(NH_3BH_3)_2$ (87 wt%), in red γ-$Mg(BH_4)_2$ (1 wt%) and in green NH_3BH_3 (12 wt%).

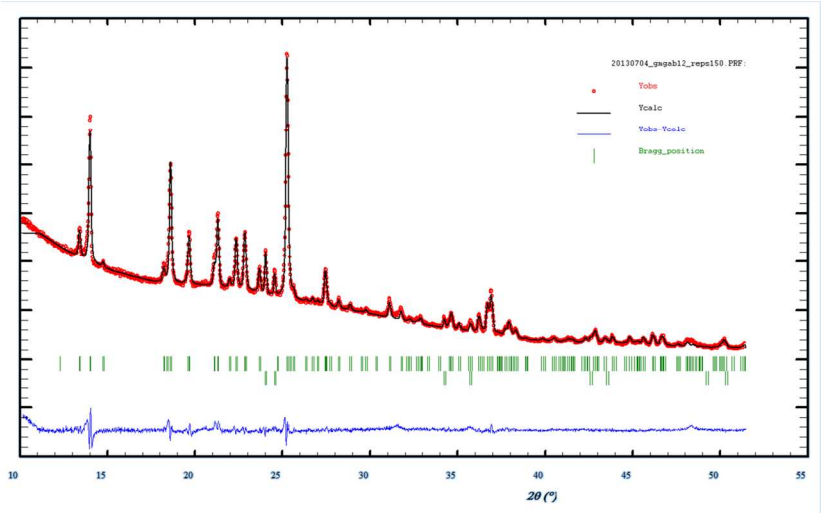

Figure S5 Rietveld refinement of PXD data for γ-$Mg(BH_4)_2$–NH_3BH_3 (1:2, s4) after 400 min BM, λ = 1.54056 Å, RT. Tic marks (top) $Mg(BH_4)_2(NH_3BH_3)_2$ (95 wt%) and NH_3BH_3 (5 wt%).

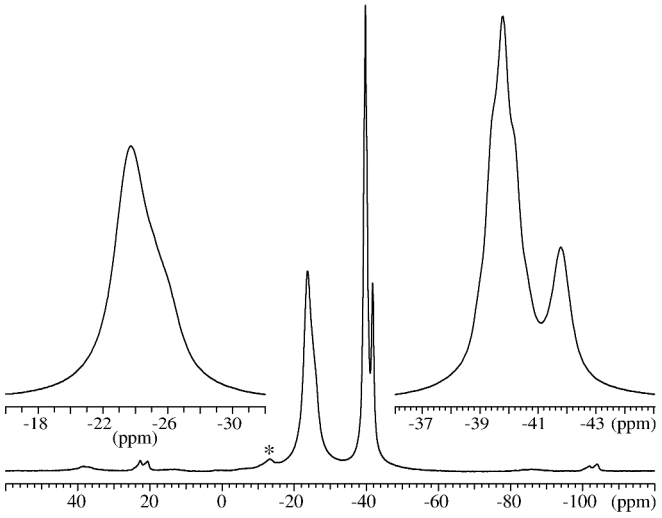

Figure S6 ^{11}B MAS NMR spectrum of a mechanochemically treated sample of γ-$Mg(BH_4)_2$–NH_3BH_3 (1:2, s4) acquired at 14.1 T using a spinning speed of ν_r = 12.0 kHz and a home-built 4 mm CP/MAS probe. The spectrum is recorded with a 0.5 μs excitation pulse ($\gamma B_1/2\pi$ = 60 kHz), a relaxation delay of 10 s and 100 scans.

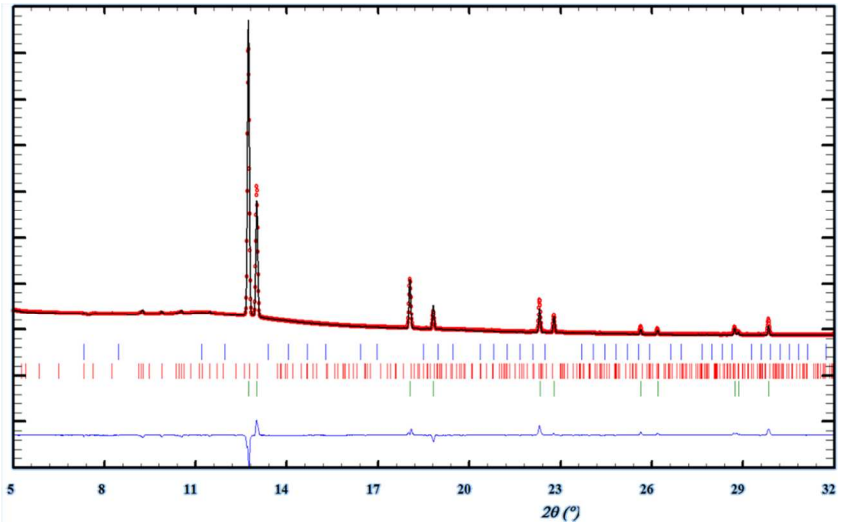

Figure S7 Rietveld refinement of PXD data for amorphous γ-$Mg(BH_4)_2$–NH_3BH_3 (1:2, s8) after compression, λ = 0.82257 Å, RT. No Bragg reflections of $Mg(BH_4)_2(NH_3BH_3)_2$ or γ-$Mg(BH_4)_2$ (blue tic marks) are observed. Small traces of α-$Mg(BH_4)_2$ are visible, while NH_3BH_3 (green tic marks) constitutes the main phase with the non-crystalline (amorphous) γ-$Mg(BH_4)_2$.

***In situ* SR-PXD investigation of the ball milling reaction between $Mg(BH_4)_2$ and NH_3BH_3 (1:2)**

Experimental: Two independent experiments were performed at ID15 beamline at ESRF, Grenoble, to compare the reactivity of α- and γ-$Mg(BH_4)_2$ with NH_3BH_3 (1:2). The setup used was identical to the one described recently [Ivan Halasz et al., *Nature Protocols* 2013, 8, 1718-1729]. Approximately 200 mg of $Mg(BH_4)_2$ and NH_3BH_3 (1:2) were loaded in a Plexiglas 14 ml jar with two 7 mm-diameter balls in stainless steel. The ball milling/diffraction experiments were performed for 99 minutes with 20 Hz milling frequency; one diffraction pattern was obtained every 12.3 seconds, resulting in 482 patterns for each milling. The wavelength (λ = 0.146687 Å) and the detector distance of 933.33 mm were determined by the CeO_2 standard packed in a capillary and LaB_6 in a 7 ml plastic jar, respectively.

Results: *In situ* SR-PXD of the ball milling process of α-$Mg(BH_4)_2$–NH_3BH_3 (1:2) are shown in Figure S8 and S9. The first obtained diffraction pattern (after 12 s of ball milling) reveals reflections from α-$Mg(BH_4)_2$, NH_3BH_3 and a single impurity peak at 1.82 ° (Figure S10). However, the impurity peak does not originate from either **1** or **2** and disappear after 13 min of ball milling. It is seen (Figure S9) that $Mg(BH_4)_2(NH_3BH_3)_2$ is formed after the 61st pattern (after 12 minutes of ball milling). There are no unidentified reflections observed from any intermediates, but the $Mg(BH_4)_2(NH_3BH_3)_2$ is formed directly from α-$Mg(BH_4)_2$ and NH_3BH_3. Rietveld refinement of SR-PXD data after 99 min of ball milling is presented in Figure S11.

In situ SR-PXD of the ball milling process of γ-$Mg(BH_4)_2$–NH_3BH_3 (1:2) is shown in Figure S12, and the conversion of γ-$Mg(BH_4)_2$ and NH_3BH_3 into $Mg(BH_4)_2(NH_3BH_3)_2$ as a function of milling time is presented in Figure S13. The first diffraction pattern after 12 seconds of milling (Figure S14) shows the reactants, γ-$Mg(BH_4)_2$ and NH_3BH_3. Formation of $Mg(BH_4)_2(NH_3BH_3)_2$ initiates after ~5 min of ball

milling and its phase fraction increases to nearly 100% after 20 minutes ball milling (Figure S13). Thus, it is concluded that under the applied conditions there are no indications of entrance of NH_3BH_3 into the pores of γ-$Mg(BH_4)_2$.

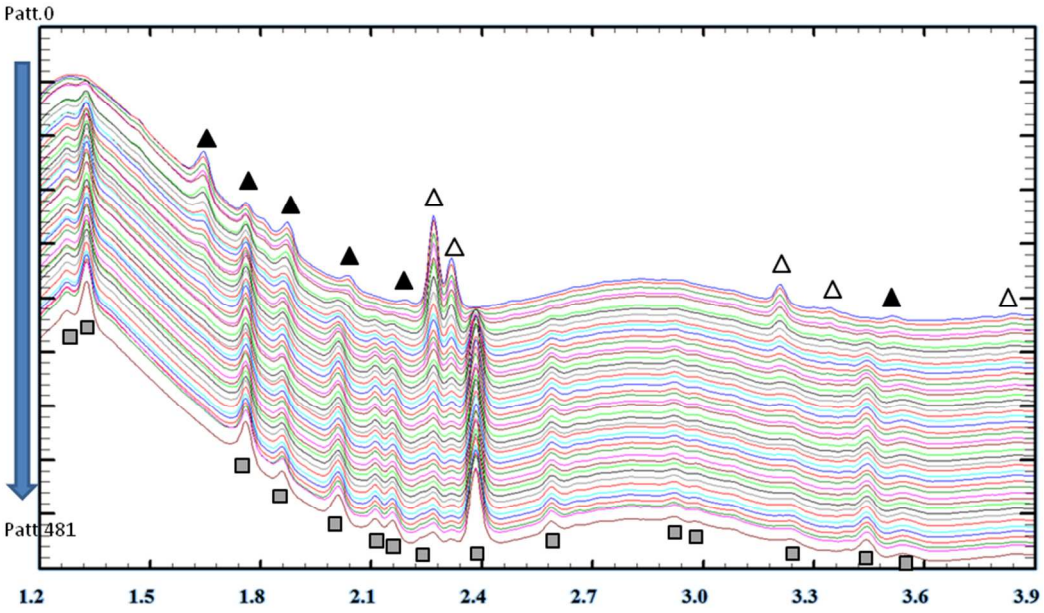

Figure S8 *In situ* SR-PXD data of the reaction between α-$Mg(BH_4)_2$ and NH_3BH_3 (1:2) every second minute (every ten's pattern is shown). The reaction evolves from top to bottom, λ = 0.146687 Å. Symbols: ▲ α-$Mg(BH_4)_2$, Δ NH_3BH_3, ◘ $Mg(BH_4)_2(NH_3BH_3)_2$.

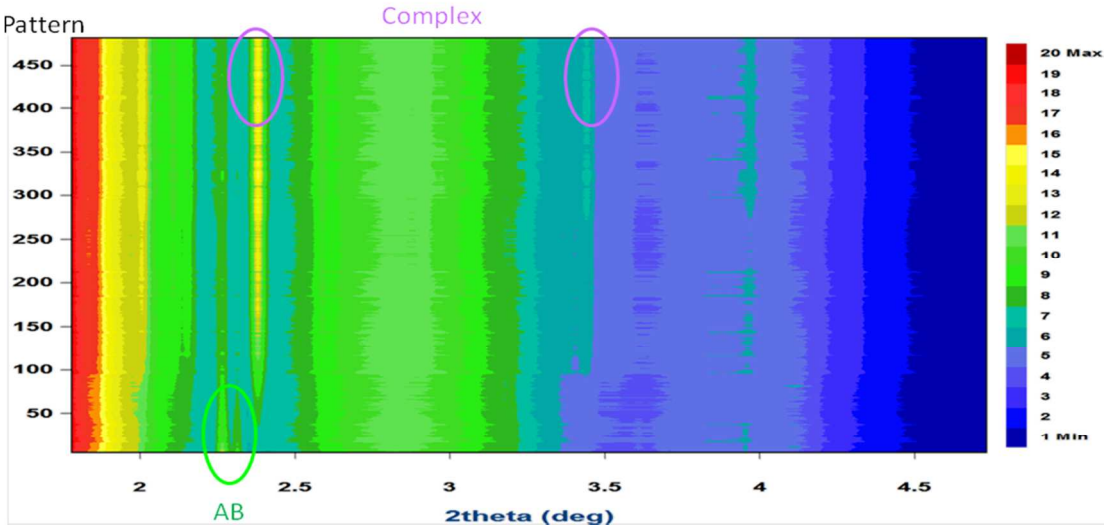

Figure S9 SR-PXD patterns collected during 99 minutes of milling for α-$Mg(BH_4)_2$–NH_3BH_3 (1:2). The relevant diffraction peaks for $Mg(BH_4)_2(NH_3BH_3)_2$ and NH_3BH_3 are highlighted by purple and green ellipses, respectively. The diffraction peaks from α-$Mg(BH_4)_2$ are difficult to distinguish as they coincide with the background generated by the plastic jar. λ = 0.146687 Å.

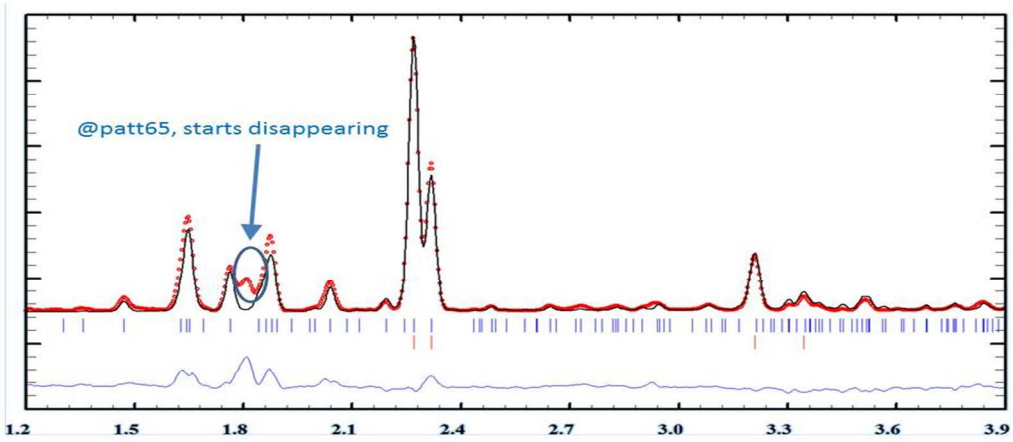

Figure S10 Rietveld refinement of the data for the first diffraction pattern (collected 12 seconds after the milling was started) for α-$Mg(BH_4)_2$–NH_3BH_3 (1:2). The background generated by the plastic jar was subtracted for clarity. Peak positions for α-$Mg(BH_4)_2$ and NH_3BH_3 are marked by blue and red

ticks, respectively. One unidentified impurity peak is observed at 1.82 °. Its intensity starts to decrease from the pattern 65 (~13 minutes of milling).

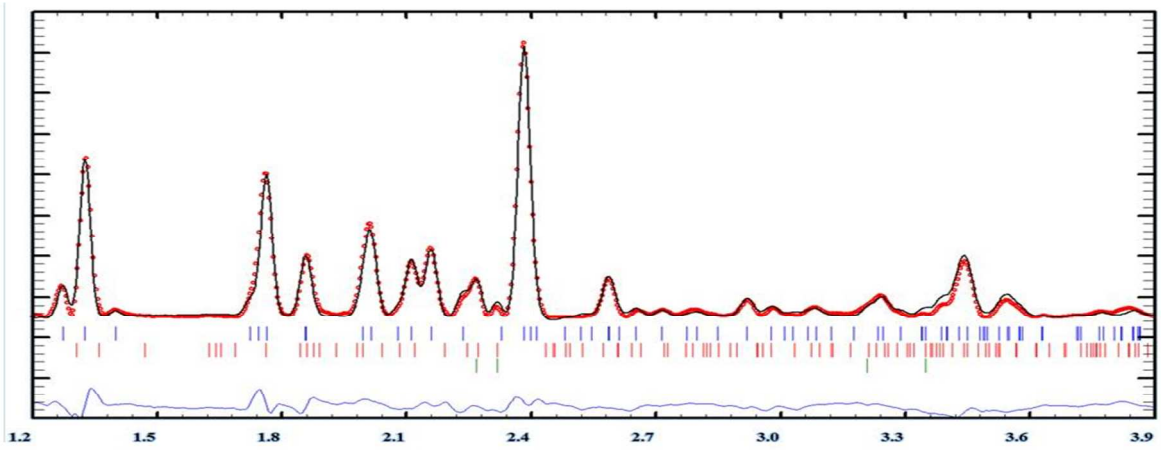

Figure S11 Rietveld refinement of the last diffraction pattern collected 99 min after the ball milling process was started for α-$Mg(BH_4)_2$–NH_3BH_3 (1:2). The background generated by the plastic jar was subtracted for clarity. Peak positions for $Mg(BH_4)_2(NH_3BH_3)_2$ (95 wt%), α-$Mg(BH_4)_2$ (0 wt %) and NH_3BH_3 (5 wt%) are marked by blue, red and green ticks, respectively.

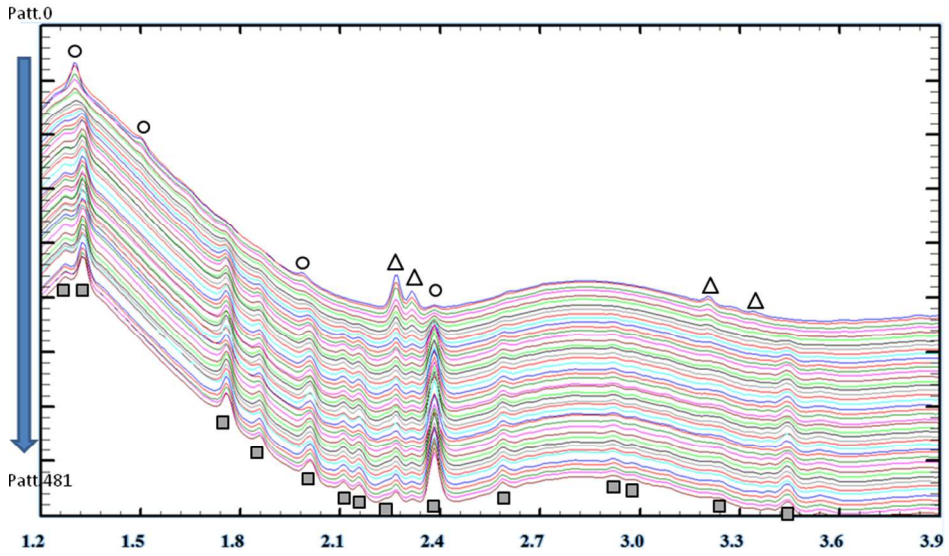

Figure S12 SR-PXD monitoring of the reaction between γ-$Mg(BH_4)_2$ and NH_3BH_3 (1:2) every two minutes (every ten's pattern is shown). The reaction evolves from top to bottom, λ = 0.146687 Å. Symbols: o γ-$Mg(BH_4)_2$, Δ NH_3BH_3, ◘ $Mg(BH_4)_2(NH_3BH_3)_2$.

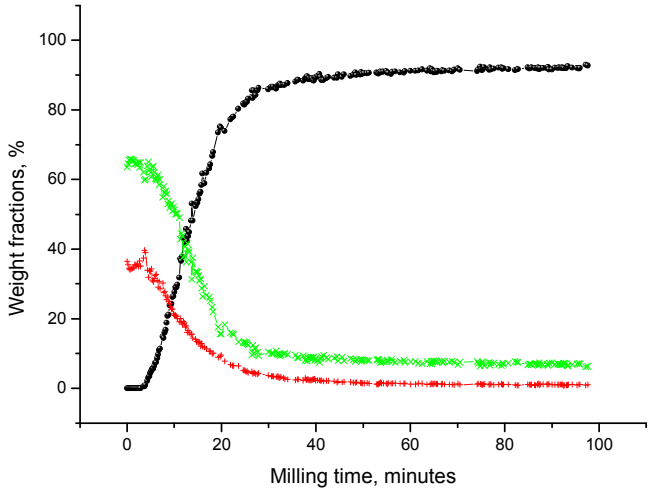

Figure S13 Evolution of the crystalline compounds as a function of ball milling time. Legend: $Mg(BH_4)_2(NH_3BH_3)_2$ (black), γ-$Mg(BH_4)_2$ (red) and NH_3BH_3 (green).

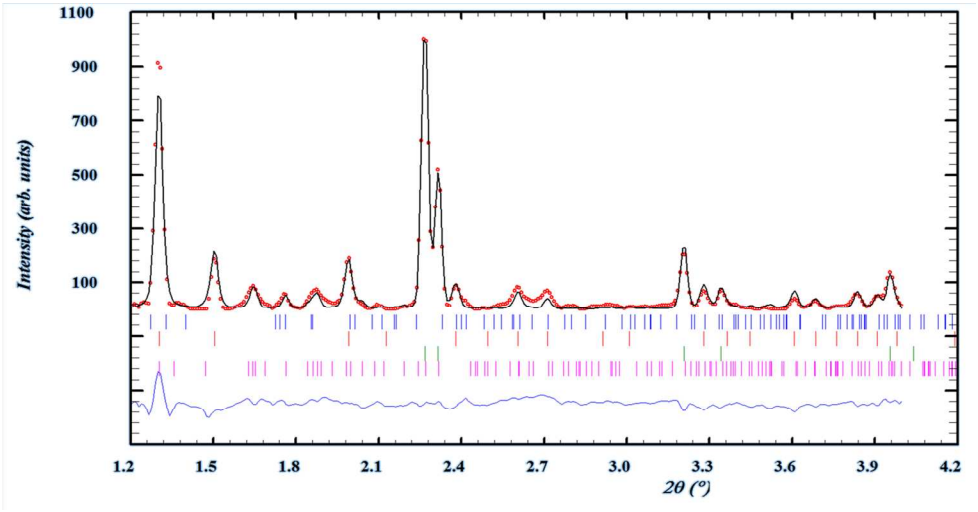

Figure S14 Rietveld refinement for the first diffraction pattern (collected 12 seconds after the milling was started) for γ-$Mg(BH_4)_2$–NH_3BH_3 (1:2). The background generated by the plastic jar was subtracted for clarity. Peak positions for γ-$Mg(BH_4)_2$ (32 wt%), NH_3BH_3 (59 wt%), $Mg(BH_4)_2(NH_3BH_3)_2$ (0 wt%) and α-$Mg(BH_4)_2$ (9 wt %) are marked by red, green, blue and pink, respectively.

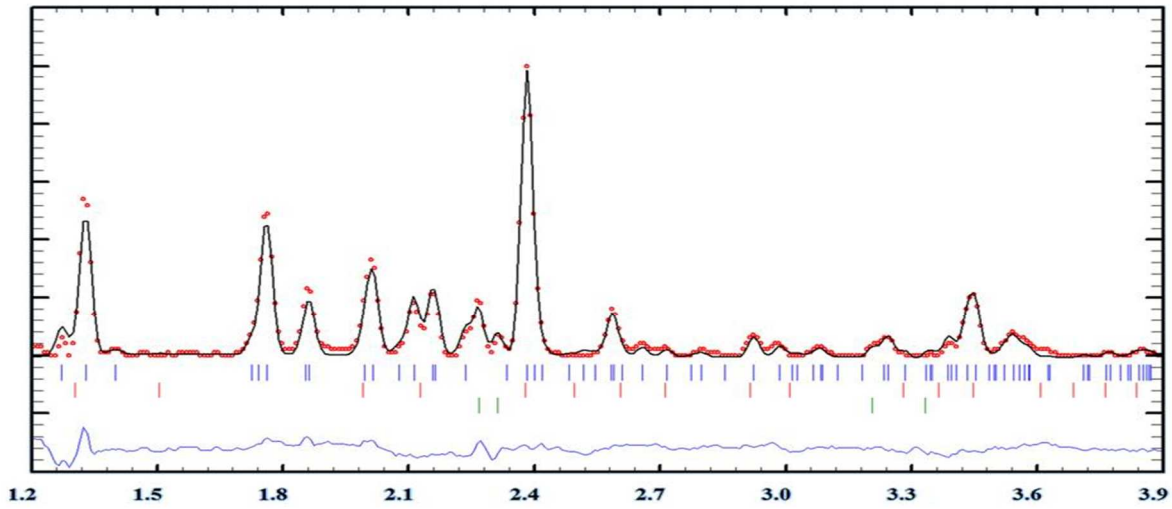

Figure S15 Rietveld refinement of the last diffraction pattern collected 99 min after the ball milling process was started for γ-$Mg(BH_4)_2$–NH_3BH_3 (1:2). The background generated by the plastic jar was subtracted for clarity. Peak positions for $Mg(BH_4)_2(NH_3BH_3)_2$ (93 wt%), γ-$Mg(BH_4)_2$ (0.5 wt %) and NH_3BH_3 (6.5 wt%) are marked by blue, red and green ticks, respectively.

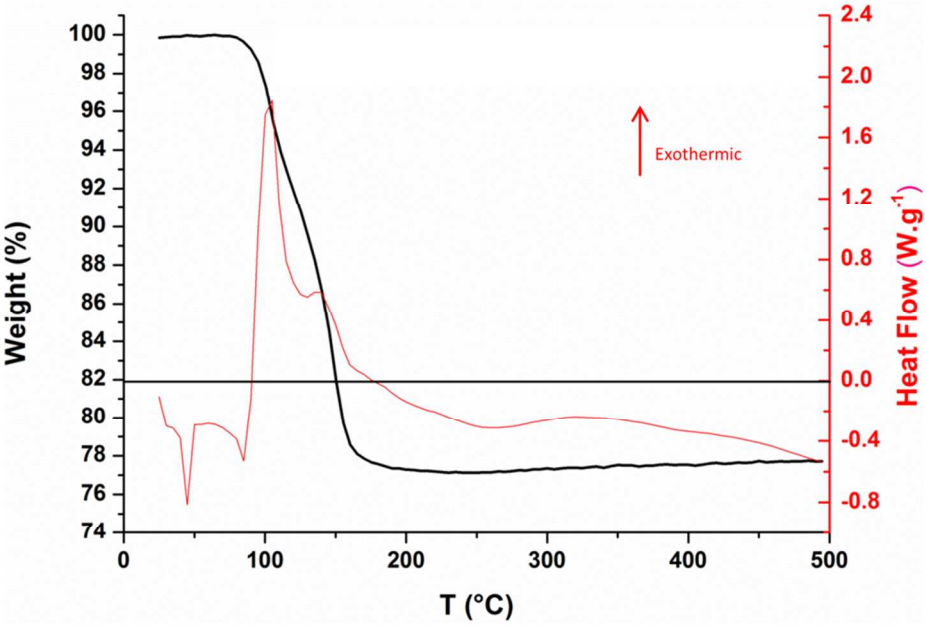

Figure S16 Thermal analysis from TGA curve (black) and DSC curve (red) of γ-$Mg(BH_4)_2$–NH_3BH_3 (1:2, s7) heated from 25 to 500 °C (5 °C/min). The sample contains some unreacted amorphous $Mg(BH_4)_2$ and NH_3BH_3.

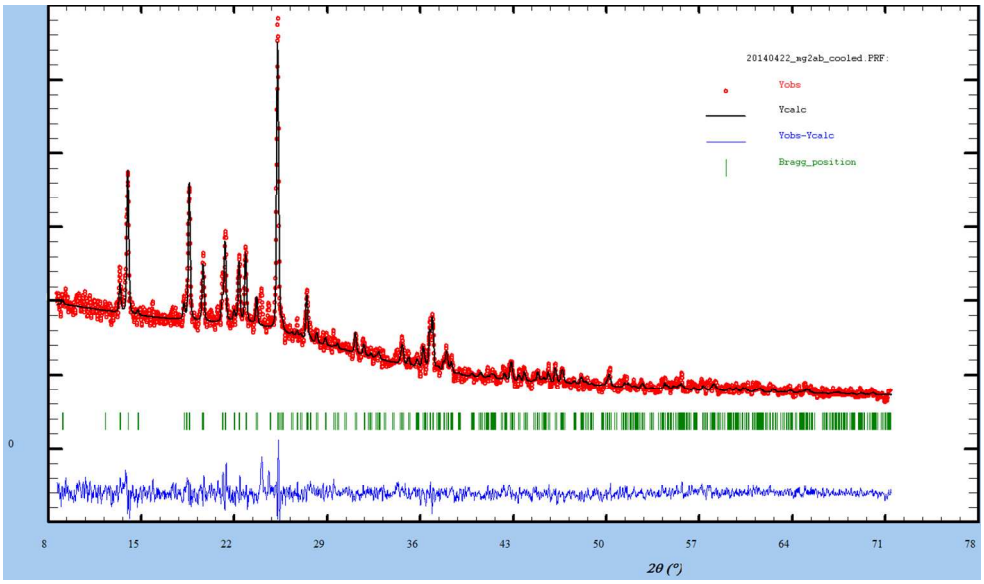

Figure S17 Rietveld refinement of $Mg(BH_4)_2(NH_3BH_3)_2$ (s2) heated to 55 °C and cooled to RT. λ = 1.54056 Å, RT. Peak positions for $Mg(BH_4)_2(NH_3BH_3)_2$ is marked by green ticks.

.

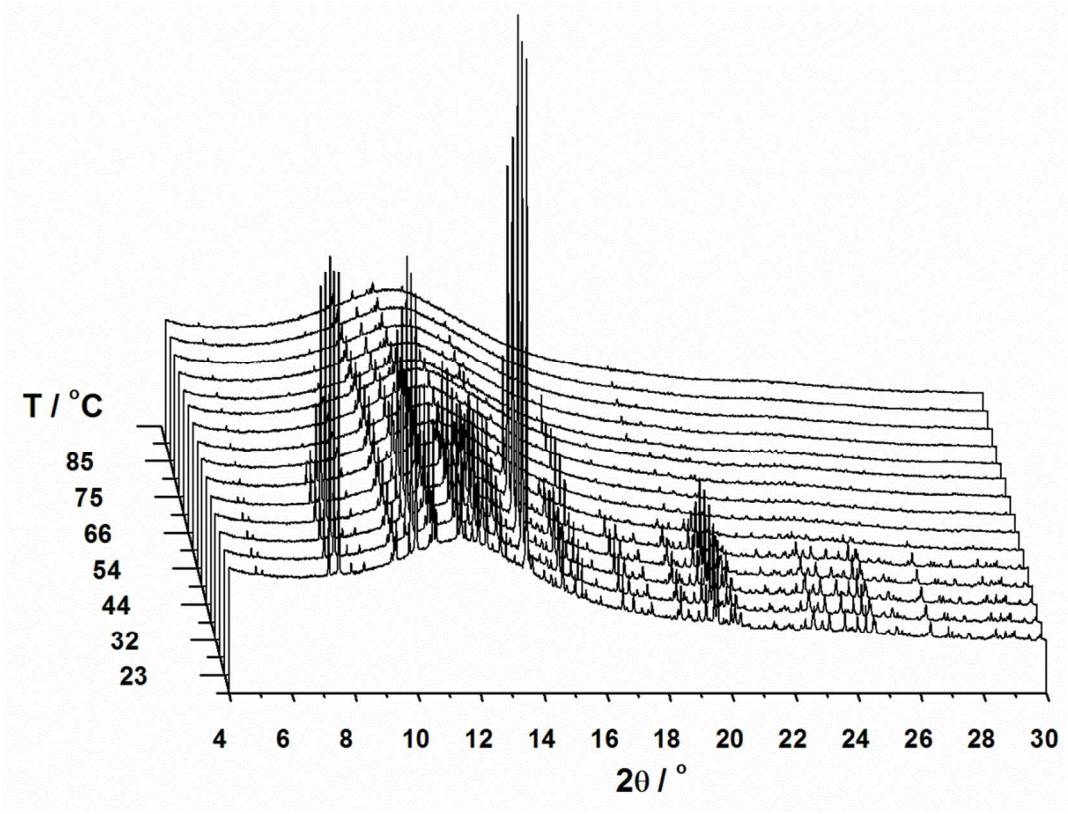

Figure S18 *In situ* SR-PXD for γ-$Mg(BH_4)_2$–NH_3BH_3 (1:0.66, s6) heated from 22 to 88 °C (4.5 °C/min, λ = 0.82712 Å, Diamond, I11). Traces of α-$Mg(BH_4)_2$ is seen at T > 45 °C after melting of $Mg(BH_4)_2(NH_3BH_3)_2$.

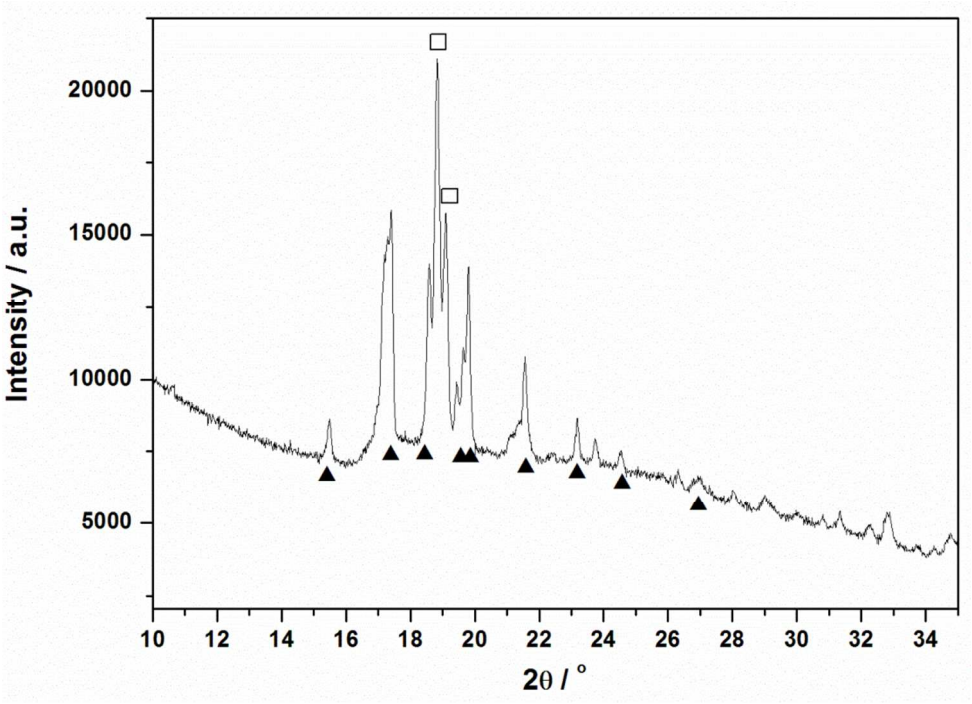

Figure S19 PXD for $Mg(BH_4)_2(NH_3BH_3)_2$ heated to 220 °C and cooled to RT, λ = 1.54056 Å.

Symbols: ▲ α-$Mg(BH_4)_2$, □ β'-$Mg(BH_4)_2$

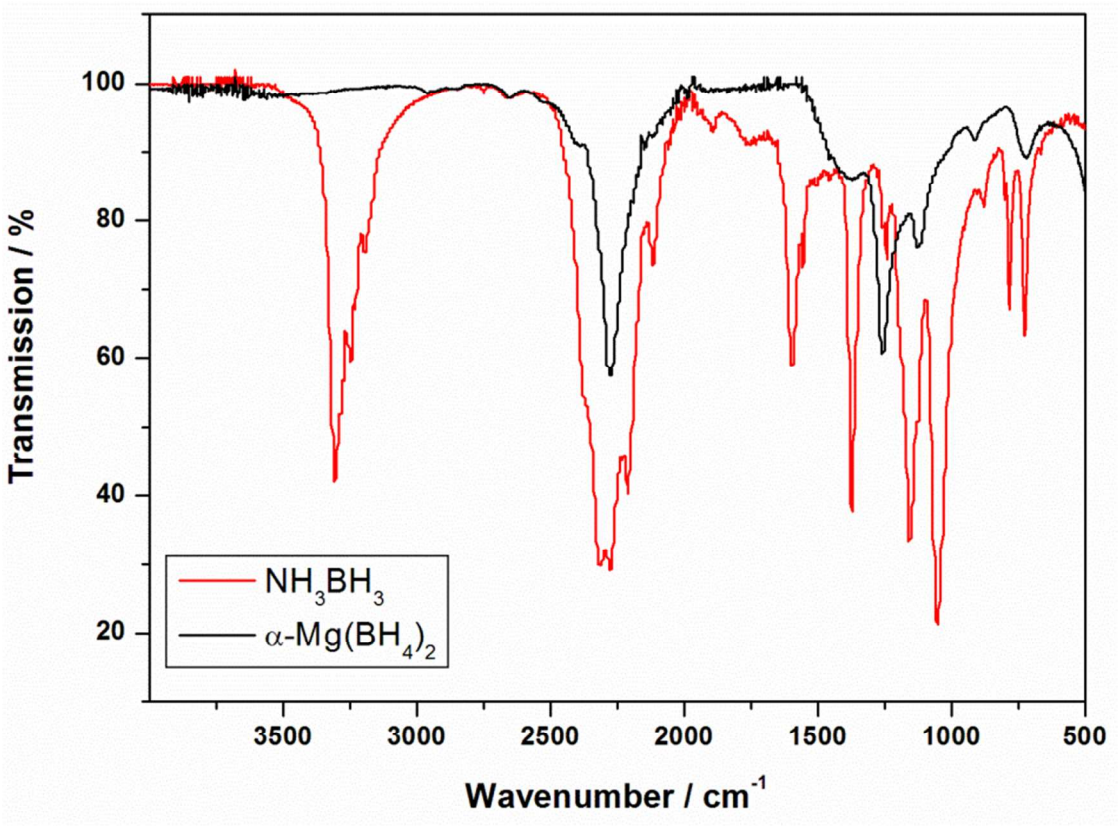

Figure S20 FTIR spectra recorded for $Mg(BH_4)_2$ (black) and NH_3BH_3 (red) at RT.

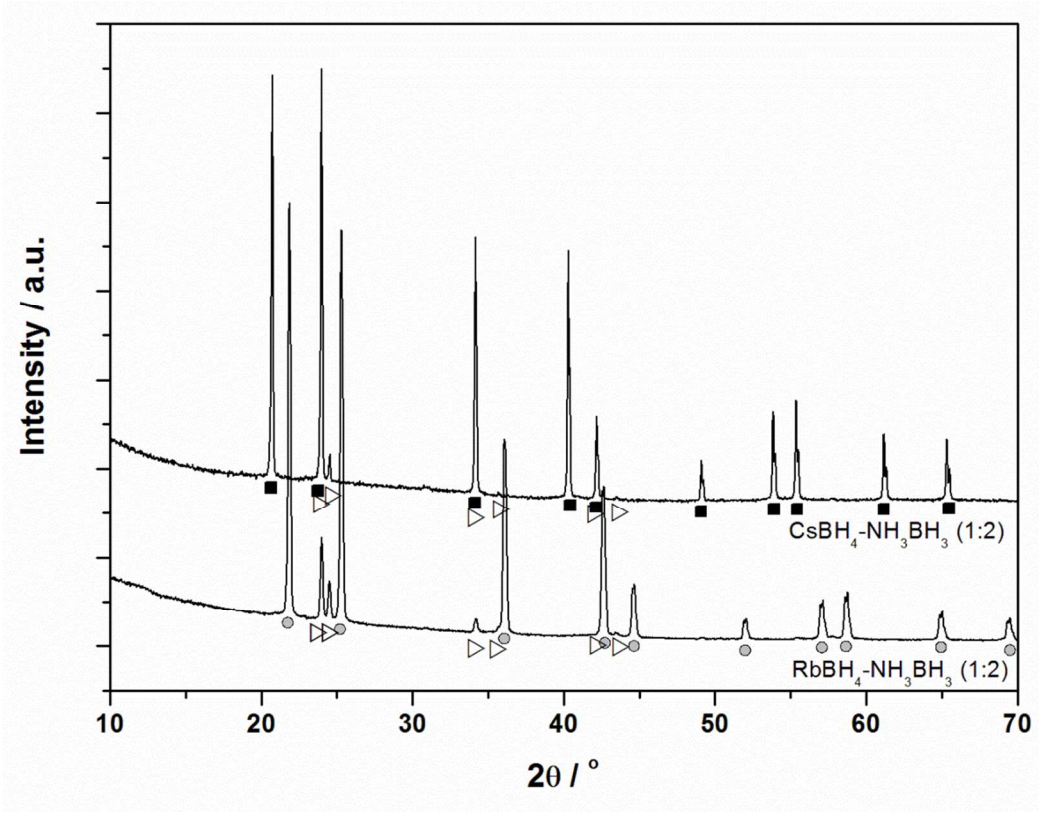

Figure S21 PXD for $RbBH_4$–NH_3BH_3 (1:2) and $CsBH_4$–NH_3BH_3 (1:2) after mechanochemical treatment, λ = 1.54056 Å. Symbols: ■$CsBH_4$, ○$RbBH_4$, ▷ NH_3BH_3